Traffic 2004; **5:** 662–671
Blackwell Munksgaard

doi: 10.1111/j.1600-0854.2004.00215.x

Toolbox

Challenges and Artifacts in Quantitative Photobleaching Experiments

Matthias Weiss
MEMPHYS-Center for Biomembrane Physics, University of Southern Denmark, Physics Department, Campusvej 55, DK-5230 Odense M, Denmark,
mweiss@memphys.sdu.dk

Confocal fluorescence recovery after photobleaching (FRAP) is today the prevalent tool when studying the diffusional and kinetic properties of proteins in living cells. Obtaining quantitative data for diffusion coefficients via FRAP, however, is challenged by the fact that both bleaching and scanning take a finite time. Starting from an experimental case, it is shown by means of computer simulations that this intrinsic temporal limitation can lead to a gross underestimation of diffusion coefficients. Determining the binding kinetics of proteins to membranes with FRAP is further shown to be severely hampered by additional diffusional contributions, e.g. diffusion-limited binding. In some cases, the binding kinetics may even be masked entirely by diffusion. As current efforts to approach biological problems with biophysical models have to rely on experimentally determined model parameters, e.g. binding rates and diffusion constants, it is proposed that the accuracy in evaluating FRAP measurements can be improved by means of accompanying computer simulations.

Key words: binding kinetics, cellular dynamics, diffusion, fluorescence recovery after Photobleaching

Received 31 March 2004, revised and accepted for publication 23 June 2004

In the last decade, our understanding of the molecular organization of living cells has undergone a dramatic change. Rather than being a deterministic, Swiss watch-like device, we realized that the cell is a very dynamic and adaptive entity with processes on various lengths and time scales. The development of confocal microscopy and the introduction of green fluorescent proteins (GFPs) as labels for different protein species have considerably helped us to gain deeper insights into the secret life and work of molecules in a living cell. In particular, the use of fluorescence recovery after photobleaching (FRAP), which was introduced in the late 1970s (1,2), has served as a powerful technique to visualize and quantify dynamic processes. Although powerful alternatives like fluorescence correlation spectroscopy have recently emerged (see (3) for an introductory review), confocal FRAP is still the most widespread approach to monitor dynamic events *in vivo*, e.g. protein diffusion and binding events (4,5). The main advantage of FRAP is its straightforward and simple strategy: after bleaching a region of interest (ROI), i.e. irreversibly destroying all fluorophores in this area, one monitors the time course of the fluorescence recovery $F(t)$. Often, just obtaining a recovery yields important insights, e.g. that two compartments exchange labeled proteins by some means. When it comes to a more quantitative evaluation of the FRAP curve, however, many subtle problems arise. The most basic question concerns the type of function one should use to fit the experimental recovery curve as this has considerable influence on the quantitative interpretation of the raw data. In particular, this 'fitting function' depends not only on the shape and area of the ROI (see (6) for an example), but also on the driving force of the recovery, e.g. diffusion, directed motion or binding events. Several studies have been devoted to this aspect, focusing, for example, on a quantitative analysis of recovery curves on nonplanar (7) or inhomogeneous (8) membranes as well as studying confined organellar geometries (9–11). Also, the influence of anomalous diffusion (12–14) has been considered in this context. So far, FRAP has been particularly useful in studying problems related to membrane traffic, e.g. the shuttling of cargo between the endoplasmic reticulum (ER) and the Golgi apparatus (15–17), the kinetics of peripheral membrane proteins which are responsible for the formation of COPI vesicles (18,19), as well as the diffusional motion of proteins in the cytoplasm (20), the mitochondria (11), the lumen of the ER (9), and on ER and Golgi membranes (21). The quantification of diffusion on membranes, however, has turned out to be a challenging task as many areas of uncertainty (e.g. the unknown geometry of the membrane) can prevent an accurate determination of the mobility (see (7,22) for a discussion on this issue). This uncertainty can be amplified to such an extent that one cannot discriminate a monomer from an oligomer consisting of hundreds of particles as the mobility on membranes only depends logarithmically on the radius of the particle's membrane-penetrating domain (23) (which, for example, can serve as a measure for the oligomeric state of a membrane protein). This example demonstrates how a high degree of uncertainty in diffusion coefficients (and/or reaction rates) can prevent a more detailed understanding of the biological system, e.g. in terms of a biophysical or computational model (for some recent references on quantitative modeling approaches see (24–27)).

With this caveat in mind, one should aim at reducing all possible sources of uncertainty when accessing dynamic

events in living cells with FRAP. It is thus worthwhile to also consider problems that are inherent to FRAP experiments. One of these intrinsic sources of error has received very little attention so far: the influence of the finite time of both bleaching and scanning. Usually, bleaching is assumed to be instantaneous when deriving fitting functions; finite-time effects of the bleaching procedure are neglected when fitting the derived theoretical expression to experimental data. It is questionable, though, whether the diffusion coefficient D_{exp} obtained by this approach really represents the actual diffusion coefficient D_{theo} of the particles of interest. As modern confocal microscopes allow one to scan a region of some 10 μm^2 in 100–200 ms, it is tempting to assume that the deviation is negligible, i.e. $D_{exp} \approx D_{theo}$. This is not obvious, however, as the ROI is often bleached in a repetitive manner, i.e. it is scanned n_{iter} times during the process to achieve a more complete bleaching. A representative example for the arising finite-time effects is shown in Figure 1, where the diffusional recovery of the ER pool of GFP-tagged GalNAc-T2 (a *trans*-membrane glycosylation enzyme which predominantly localizes to the Golgi apparatus) has been monitored. The same circular ROI was bleached with $n_{iter} = 2$, 5, 10 scanning iterations on the very same cell (between the different bleaches the cell was given some minutes to recover and reach the steady state again). As can be seen from Figure 1, the half time ($t_{1/2}$) of the recovery increased considerably when the number of scanning iterations during the bleach (n_{iter}) was increased. In fact, the diffusion coefficient that one would derive from these curves decreases *systematically* from $D_{exp} \approx 2\,\mu m^2/s$ ($n_{iter} = 2$) to $D_{exp} = 0.7\ \mu m^2/s$ ($n_{iter} = 10$), an effect which also persists when averaging over many cells. The purpose of this paper is to elucidate when and under which circumstances these finite-time effects arise and become important when performing FRAP experiments to access diffusion coefficients. Using computer simulations, it is shown here that in typical FRAP scenarios, diffusion coefficients are generally underestimated about two- to fourfold. In contrast, access to the binding kinetics of peripheral membrane proteins with FRAP measurements is less affected by this finite-time effect. However, in this FRAP application, diffusional contributions from the membrane and the cytoplasm can mask the binding kinetics entirely, rendering the elucidation of the kinetic rates impossible. Based on these findings, it is advisable to always combine FRAP experiments with appropriate computer simulations rather than performing simple fitting. This more elaborate approach will considerably improve the data accuracy and interpretation in terms of a biophysical model.

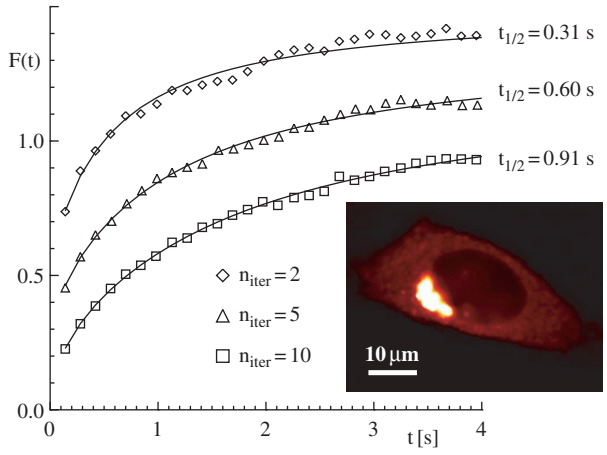

Figure 1: Example of finite-time effects when determining diffusion coefficients with FRAP. Performing FRAP on the ER-pool of the Golgi protein GalNAc-T2 and using the same circular ROI (area 11 μm^2) but bleaching it in $n_{iter} = 2$, 5, 10 scanning iterations (◇, △, □, respectively) yields strongly varying recovery times ($t_{1/2}$). During the data acquisition, only the ROI in the ER was imaged to improve the temporal resolution. The recovery curves were fitted using eqn. 2 (full lines) in the range $t \leq 8$ s (for better visibility only the range $t \leq 4$ s is shown). The determined diffusion coefficients showed considerable variations ($D_{exp} \approx 2\ \mu m^2/s$, $1\ \mu m^2/s$, and $0.7\ \mu m^2/s$, respectively). For better visibility the FRAP curves have been shifted vertically. Inset: The used HeLa cells stably express GalNAc-T2 and show a prominent Golgi staining with a dimmer fluorescence in the ER.

Results and Discussion

When the fluorescence recovery in FRAP experiments is due to diffusion of labeled particles into the ROI, the major goal typically is to extract a diffusion coefficient D_{exp} from the experimental data, i.e. to measure the molecular mobility. To accomplish this, an appropriate formula is fit to the recovery data from which one can derive a quantitative estimate for D_{exp} that ideally equals the real diffusion coefficient D_{theo} of the molecule under study. To obtain the formula used for fitting the data, one usually has to assume that the bleaching is instantaneous. Thus one can expect that the extracted D_{exp} deviates from the actual coefficient D_{theo}. An example for this is shown in Figure 1, where the diffusion coefficient of a membrane protein in the ER has been determined by different FRAP protocols, i.e. the ROI has been repetitively scanned n_{iter} times during the bleaching. As a result, the estimate of the diffusion coefficient D_{exp} decreases approximately threefold when n_{iter} is increased. To quantify and further characterize these deviations, computer simulations of FRAP have been performed on a square lattice with the typical lateral dimensions of HeLa cells (33 $\mu m \times 33\ \mu m$). Unless stated otherwise, a circular ROI (radius $r = 2\ \mu m$) located in the center was bleached either instantaneously or at the bleaching rate γ in n_{iter} scanning iterations (see Methods for details). Fitting was performed with an expression derived for circular regions ((6), see also eqns. 2 and 3, Methods).

First, the influence of the number of bleaching iterations n_{iter} was investigated. To this end, the bleaching rate $\gamma = 1/150\ ms^{-1}$, i.e. the laser intensity, was kept constant

and the actual diffusion coefficient of the particles was fixed to $D_{theo} = 1\ \mu m^2/s$, which is a representative value for diffusion of a protein on a membrane when estimating the mobility via the Saffman–Delbruck equation (23) (see also Methods). In Figure 2A, representative recovery curves for $n_{iter} = 3$, 10 are shown together with the one obtained for an instant bleaching ('control curve'). Also shown are best fits according to eqn 2. While the fitting of the control curve confirmed the theoretical diffusion coefficient ($D_{exp} = D_{theo} = 1\ \mu m^2/s$), the extracted diffusion coefficients for $n_{iter} = 3$, $n_{iter} = 10$ are much smaller than anticipated, namely $D_{exp} = 0.63\ \mu m^2/s$ and $D_{exp} = 0.39\ \mu m^2/s$. This deviation, i.e. the ratio D_{exp}/D_{theo}, is in good agreement with the observations made *in vivo* (see Figure 1). The increase of the deviation with increasing n_{iter} can be understood by closely inspecting the postbleach fluorescence pictures and their lateral cross-sections (Figure 2B–D). Essentially, D_{exp} is given by the ratio of the radius r of the bleached ROI (here: $r = 2\ \mu m$) and the typical recovery time T obtained from fitting the time course of the recovery (see eqn. 3, Methods). However, diffusion does not stop while repetitively bleaching the ROI n_{iter} times, i.e. particles that are bleached in the first scan have time to leave the ROI, and unbleached ones can enter the ROI from the rims and are subsequently bleached. Due to this, a 'corona' of bleached particles is formed around the ROI. This depletion zone effectively increases the time T needed for the recovery. On the other hand, as the size of the actually bleached region cannot be quantified properly, one simply assumes that only the ROI with radius r has been bleached. Due to the increase in T this eventually leads to a lower ratio r^2/T, which determines D_{exp}, and one thus underestimates the diffusion coefficient. In contrast to real experiments, the growth of the ROI due to this 'corona effect' can be easily observed in FRAP simulations. Figure 2B–D shows the bleached regions and the cross-sections associated with the recovery curves in Figure 2A. For the control curve (instant bleaching,

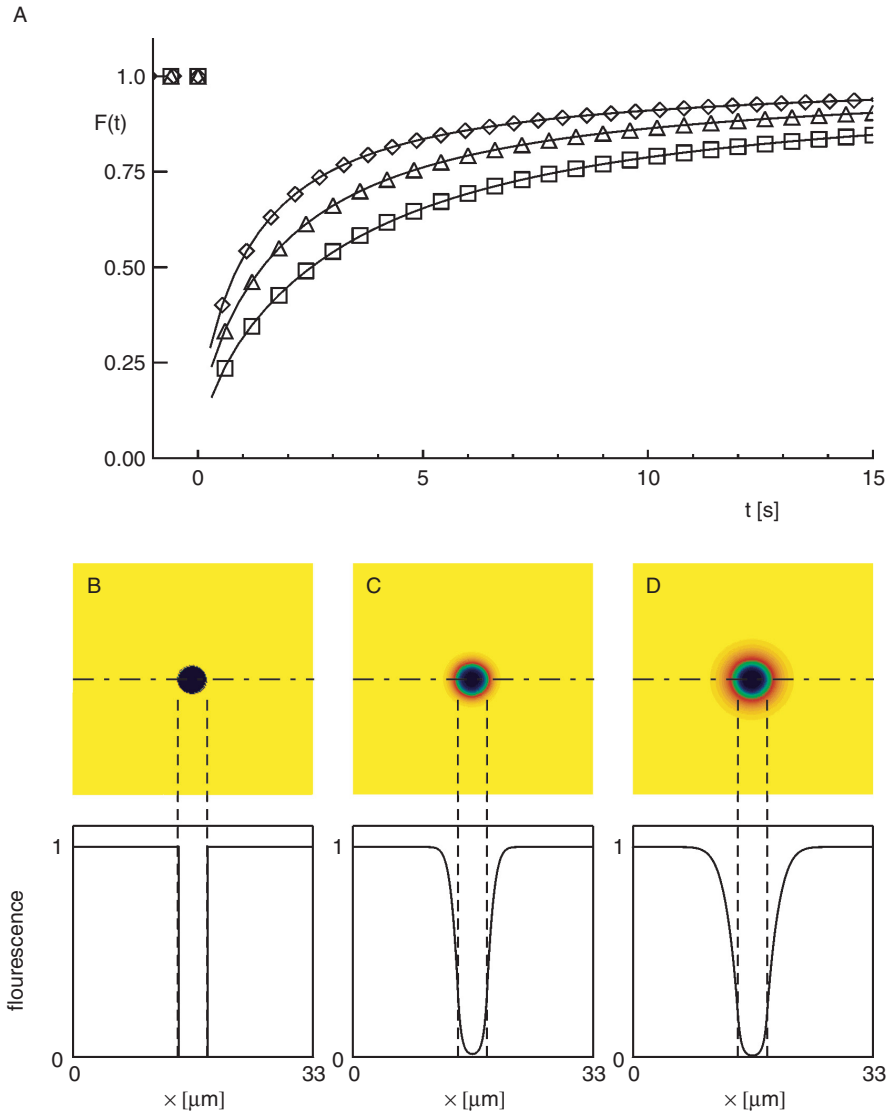

Figure 2: The formation of a bleached 'corona' limits the precision when evaluating FRAP curves. A) Recovery curves *F(t)* after bleaching a circular ROI ($r = 2\ \mu m$) instantaneously (◇), and in $n_{iter} = 3$ (△) and $n_{iter} = 10$ iterations (□) at the rate $\gamma = 1/150\ ms^{-1}$. Full lines are best fits according to eqn. 2 (Methods) and yield diffusion coefficients $D_{exp} = 1\ \mu m^2/s$, $D_{exp} = 0.63\ \mu m^2/s$ and $D_{exp} = 0.39\ \mu m^2/s$, respectively. The deviation from the diffusion coefficient $D_{theo} = 1\ \mu m^2/s$ imposed in the simulations is explained by inspecting the corresponding postbleach fluorescence densities (upper panel; yellow: high fluorescence) and cross-section profiles (lower panel) for an instantaneous (B) and stepwise bleaching (C, $n_{iter} = 3$; D, $n_{iter} = 10$). As can be seen from the cross-section profiles (taken along the indicated dash-dot line), the bleached spot broadens with increasing n_{iter} and a bleached 'corona' emerges around the specified ROI (dashed lines). This 'corona effect' leads to the decrease of D_{exp} as quantified from the recovery curves in A (see main text for details).

Figure 2B) the bleached region is simply the ROI, i.e. a circle of radius $r = 2\,\mu m$ with a sharp, step-like transition in the fluorescence between the bleached and the nonbleached parts of the cell. In contrast, bleaching with a finite rate for $n_{iter} = 3$, 10 times leads to a broadening of the bleached region beyond the marked ROI (Figures 2C,D) due to the 'corona effect'. In these cases, the rims of the actually bleached region are not as steep as for instantaneous bleaching but appear sigmoidally smoothed.

To further quantify the corona effect, several bleach rates γ and iteration numbers n_{iter} have been used for simulations while keeping the imposed diffusion coefficient $D_{theo} = 1\ \mu m^2/s$ fixed. The resulting recovery curves were fitted using eqn. 2 and the obtained recovery time T was used in combination with the radius $r = 2\,\mu m$ of the ROI to determine the diffusion coefficient D_{exp} via eqn. 3. The obtained diffusion coefficients are shown in Figure 3A as a function of the number of iterations, n_{iter}. One can clearly observe a decrease of the diffusion coefficient D_{exp} with increasing numbers of bleach iterations which levels off at $D_{exp} \approx 0.25 \cdot D_{theo}$ for large n_{iter}. This means that it is easy to underestimate the diffusion coefficient in FRAP applications about fourfold when picking an unfortunate number of bleaching iterations. For measurements on membranes, this error can give rise to gross misinterpretations, e.g. when trying to estimate the (oligomeric) size of membrane proteins or raft-like domains (see above and discussion in (22)). Interestingly, the bleaching rate γ, i.e. the laser intensity, only plays a minor role here, as different γ gave rise to almost the same functional dependence $D_{exp}(n_{iter})$. This result did not change when bleaching an alternative geometry (square ROI) or when the area of the ROI was increased (Figure 3A). Also, incomplete bleaching (instantaneous or with a finite rate γ) did not alter the results in the simulations (data not shown). In real FRAP experiments, however, incomplete bleaching can prevent accurate determination of the diffusional mobility. Most of the dynamic information is contained in the early recovery at times $t < 3 \cdot t_{1/2}$ where *F(t)* strongly depends on time and incomplete bleaching reduces the number of these valuable data points before the saturation. This hampers the proper evaluation of the dynamics due to uncertainties in the fitting procedure.

As a next step, the imposed diffusion coefficient D_{theo} was varied over a wide range while keeping the bleaching rate γ and the number of iterations n_{iter} fixed. In fact, the interval of tested diffusion coefficients covered the range from fast diffusion in cytoplasm ($D_{theo} \approx 15\ \mu m^2/s$) to slow diffusion on membranes ($D_{theo} \approx 0.1\ \mu m^2/s$). The numerically obtained recovery curves were fitted as before and the ratio $\eta = D_{exp}/D_{theo}$ was plotted as a function of D_{theo}. As anticipated, a decrease of the ratio η is observed for increasing D_{theo} which levels off at different, yet fairly low, values depending on the chosen bleaching rate and iteration number (Figure 3B). As a rule of thumb, one can say that the ratio η deviates from unity when increasing

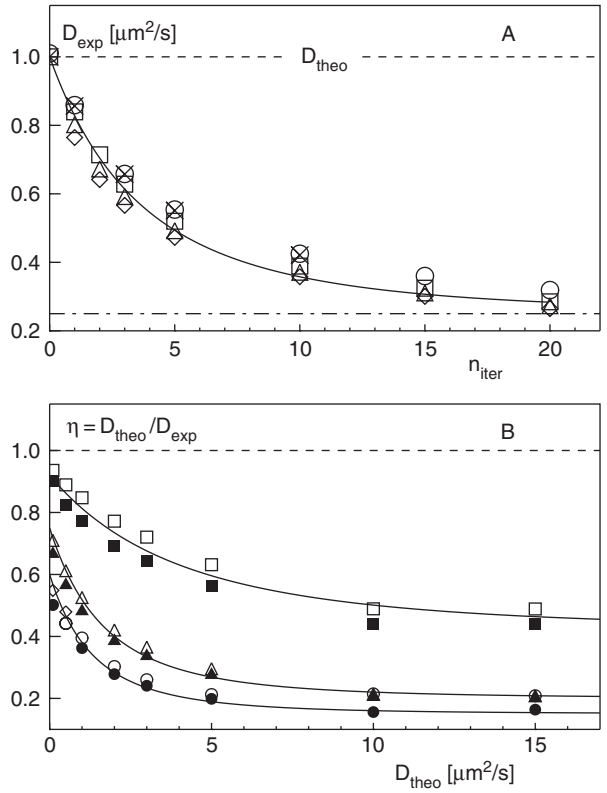

Figure 3: Diffusion coefficients are underestimated due to the 'corona' effect. A) Increasing the number of bleach iterations n_{iter} leads to a decrease of the diffusion coefficient D_{exp} as obtained from fitting the recovery curves *F(t)* with eqn. 2. The diffusion coefficient imposed in the simulations was $D_{theo} = 1\ \mu m^2/s$, i.e. D_{exp} can become 4–5 times smaller than the anticipated value D_{theo}. Symbols indicate various bleaching conditions (◇, △, □: circular ROI [radius 2 μm], bleach rates $\gamma = 1/150\,ms^{-1}$,2/150 ms^{-1}, 4/150 ms^{-1}; ○: ROI [radius 2.5 μm], $\gamma = 1/150\,ms^{-1}$; ×: square ROI [area 16 μm^2], $\gamma = 1/150\,ms^{-1}$). B) Due to the corona effect, the ratio $\eta = D_{exp}/D_{theo}$ decreases with increasing D_{theo}, n_{iter} and γ, as this promotes the formation of a zone around the bleach spot which is depleted of fluorescent particles. Open, closed symbols: $\gamma = 1/150\,ms^{-1}$, 4/150 ms^{-1}; □, ■: $n_{iter} = 1$, △, ▲: $n_{iter} = 5$, ◇, ◆: $n_{iter} = 10$. Full lines are phenomenologic spline fits to guide the eye.

the number of iterations n_{iter} and/or the imposed diffusion coefficient D_{theo}. Any increase in these parameters leads to an enhancement of the corona effect.

It might be expected that the 'corona' effect could be circumvented by using a higher laser intensity, which helps to reduce the number of bleaching iterations, n_{iter}. Even a single scan, however, can already lead to considerable deviations (cf. Figure 3). It is therefore better to aim at reducing the time of the scanning, i.e. the photon integration time per pixel. This strategy, however, is constrained not only by the limited speed of the confocal scan head, but also by the fact that a shorter integration time per pixel can lead to incomplete bleaching (cf. the above caveat) and the enhancement of fluctuations in the fluorescence

during the data acquisition (which decreases the accuracy of the fitting afterwards). In general, the choice of the FRAP parameters depends very much on the studied problem and the used setup, but one should always aim at a strong bleaching in a short time, while at the same time keeping the fluctuations in the signal low enough to allow a successful fitting. Readers interested in the related technical aspects can consult the extensive literature on FRAP (see (28), and (5) for an introduction). The most straightforward approach to quantify (and extract) the 'corona' effect is to supplement FRAP measurements with computer simulations (similar to those presented here). The following may be a more practical and universal procedure. The experimental values D_{exp} (averaged over many cells) are gathered for different bleach iterations n_{iter} and these values are plotted as shown in Figure 3A. From this plot, it is possible to extrapolate the value $n_{iter} = 0$, which gives a reasonable estimate for D_{theo}. An alternative method, e.g. fluorescence correlation spectroscopy (for an introductory review see (3)) can also be used to determine the actual diffusional mobility more accurately.

As FRAP is also frequently used to assess the binding kinetics of peripheral membrane proteins to target membranes (for recent examples see (18,19)), it was natural to ask whether the quantification of these events is sensitive to intrinsic sources of uncertainties as well. In contrast to the previous case of diffusion-mediated recovery, here the FRAP curve should be described by a single exponential recovery with typical recovery rate $\omega_{theo} = k_{on} + k_{off}$ if binding events are dominant. Fitting the experimental data (eqn. 4, Methods), the aim is to determine ω_{exp}. Ideally ω_{exp} should equal ω_{theo} and thus yield information about the reaction rates k_{on} and k_{off}. Two different settings have been considered to investigate the sensitivity of FRAP experiments when trying to elucidate the binding kinetics to a membrane target: the protein can exist in a cytosolic and a membrane-bound form and binds (unbinds) with rates $k_{on}(k_{off})$ (*i*) everywhere on the membrane or (*ii*) only in the ROI. The former scenario thus describes a spatially uniform binding/unbinding cycle of a peripheral membrane protein, e.g. the binding of the small GTPase ARF-1 to Golgi membranes (18,19). Scenario *ii*, on the other hand, models the binding and arresting of a peripheral protein to a specialized domain on the membrane, e.g. the binding of COPII proteins to exit sites of the ER (29,30). With regard to these examples, the cytoplasmic diffusion coefficient was taken to be $D_{theo} = 10\ \mu m^2/s$; for membrane diffusion, $D_{theo} = 1\ \mu m^2/s$ was used in scenario *i*. In scenario *ii*, diffusion on the membrane was prohibited.

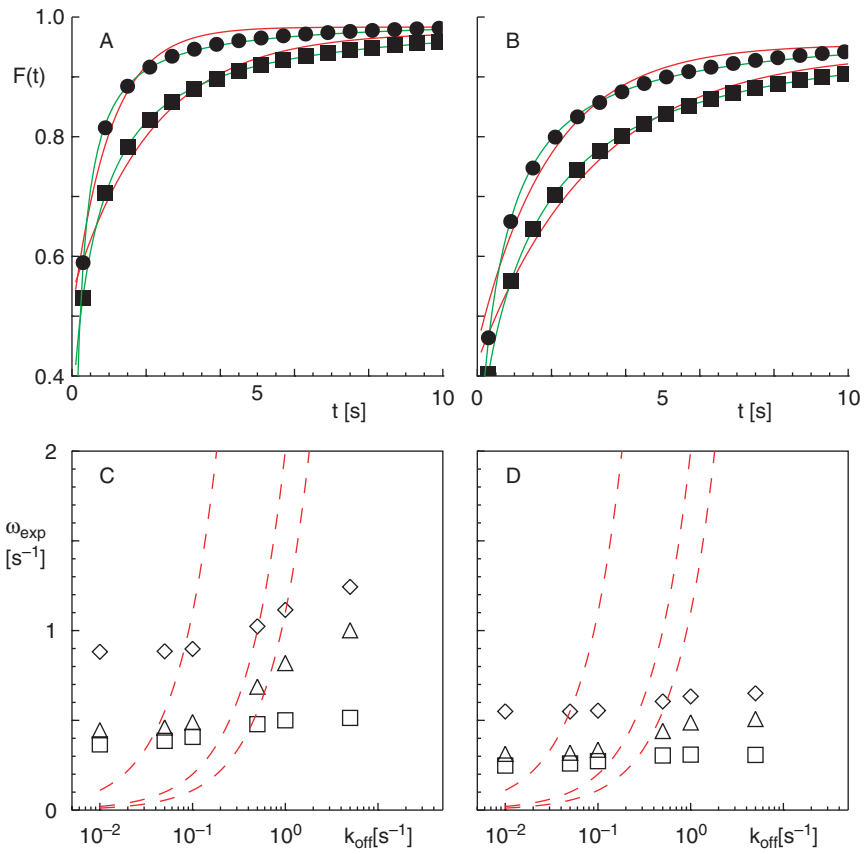

Figure 4: The spatially uniform binding kinetics of a peripheral membrane protein is masked by diffusion. A) The recovery after instantaneously bleaching a circular ROI ($r = 2\ \mu m$) is carried by cytoplasmic and membrane diffusion ($D_{theo} = 10\ \mu m^2/s$ and $D_{theo} = 1\ \mu m^2/s$, respectively) as well as by a uniform binding/release to/from the membrane at rates of $k_{on} = k_{off} = 0.05/s$ (●) and $k_{on} = k_{off} = 5/s$ (■). Best fits with a model for binding (eqn. 4, red full lines) describe the data poorly, i.e. they show a visible deviation from the data. A better, though meaningless, fit is obtained when using eqn. 2 for a diffusive recovery (green full lines). B) Same as in A when the bleaching was performed with $n_{iter} = 1$ iteration and bleach rate $\gamma = 1/150\ ms^{-1}$. C) Using instantaneous bleaching, the recovery rate ω_{exp} as obtained by fitting *F(t)* with the model for recovery due to binding (eqn. 4) shows almost no dependence on the imposed binding kinetics (◇: $k_{on} = 0.1k_{off}$, △: $k_{on} = k_{off}$, □: $k_{on} = 10k_{off}$). The anticipated recovery rates ω_{theo} (red dashed lines), which are determined by the binding kinetics, are not reflected in ω_{exp}. D) Same as in C when bleaching with $n_{iter} = 5$ and $\gamma = 1/150\ ms^{-1}$. Please note that the abscissas in C and D have a logarithmic scale, whereas the ordinates are linear. Scales on ordinates are the same within each panel.

To match the scenario in real experiments, the bleached ROI (circular, $r = 2\,\mu m$) not only contained parts of the target membrane but also some fraction of the adjacent cytoplasm (see Methods for details). Thus, rather than the previously described 'corona effect', the major source of uncertainty here can be expected to arise from the competition of the typical time scales needed for the diffusion towards the target and the subsequent binding to it. In other words, even for instantaneous bleaching, the pure binding model (eqn. 4) may fail to describe the FRAP curve.

Let us first concentrate on scenario *i*, a uniform attachment/detachment in the presence of cytoplasmic and membrane diffusion. Figure 4 shows representative examples of the recovery when the binding and unbinding occurs at the same rates when bleaching was instantaneous (Figure 4A) or occurred within $n_{iter} = 5$ iterations with a bleaching rate $\gamma = 1/150\,ms^{-1}$ (Figure 4B). In all cases, a fitting with the formula for a recovery due to binding (eqn. 4, Methods) provided a poor description of the data (Figure 4A,B). This result was not altered when the binding and unbinding rates differed 10-fold either way ($k_{on} = 0.1k_{off}$ and $k_{on} = 10k_{off}$) or when the kinetic rates were changed within a reasonable range ($k_{off} = 0.01$–$10/s$). These findings are summarized in Figure 4 (C,D) for different bleach protocols (C: instantaneous bleaching, D: $n_{iter} = 5$, $\gamma = 1/150\,ms^{-1}$). In fact, the recovery rate ω_{exp} as obtained from fitting the FRAP curves with eqn. 4 shows hardly any dependence on k_{on} and k_{off}, i.e. ω_{exp} deviates strongly from the expected value $\omega_{theo} = k_{on} + k_{off}$ (red dashed lines in Figure 4C,D). The reason for the observed discrepancy between ω_{theo} and ω_{exp} is easily explained: the recovery into the bleached ROI is not only carried by binding events but also by diffusion in the cytoplasm and on the membrane (with diffusion coefficients $D_{theo} = 10\,\mu m^2/s$ and $D_{theo} = 1\,\mu m^2/s$, respectively). These two events set the dominant time scales for the entire recovery and therefore completely mask the binding event. Fitting the experimental FRAP curves with a combination of the formulas for diffusive (eqn. 2) and reaction-driven (eqn. 4) recovery might be expected to improve the determination of the binding kinetics. But it turns out that in this case the contribution of the diffusion will dominate the fitting and the kinetic rates will be left obscured. Moreover, diffusion towards the target and the subsequent binding to it are sequential events. Simply adding eqns. 2 and 4 is therefore generally not valid, since this approach assumes that the diffusion and binding are independent events. Hence, one can infer from these results that by fitting FRAP curves using eqn. 4 one often cannot assess the uniform binding kinetics of a peripheral membrane protein as this information is masked by diffusion.

Even if the binding kinetics is masked, one can still determine whether an observed recovery is due only to diffusion or whether binding kinetics is also involved. If diffusion is the only contributor to the recovery, an increase in the area A_{ROI} of the ROI will lead to an increase in the recovery $t_{1/2}$ by the same factor (cf. eqn. 3, Methods). Recovery due to binding does not depend on A_{ROI}. By testing the dependence of $t_{1/2}$ on the bleached area A_{ROI} it is possible to test for the presence of masked binding events (31,32). Indeed, when using the same kinetic parameters as in Figure 4 and plotting the ratio $t_{1/2}/A_{ROI}$ as a function of the binding rate ($k_{on} = k_{off}$), one can see in Figure 5 that the data points do not collapse to a single curve (as one would anticipate for a purely diffusive recovery) but they deviate from each other for increasing A_{ROI}. The observed decrease of the ratio $t_{1/2}/A_{ROI}$ for increasing A_{ROI} is consistent with the expectation that a binding event is involved even when it is difficult to quantify its kinetics.

Let us now turn to scenario *ii,* the specific binding to a specialized subdomain which captures the protein and prevents it from diffusing on the membrane. Here, the results are substantially different. As can be seen from the representative examples in Figure 6A,B, the fitting using eqn. 4 (recovery due to binding kinetics) yields a good description of the numerical data. Remarkably, this holds true for instantaneous as well as stepwise bleaching ($n_{iter} = 5$, $\gamma = 1/150\,ms^{-1}$). Plotting the obtained recovery rate ω_{exp} as a function of the imposed unbinding rate k_{off} and also varying the binding rate ($k_{on} = 0.1k_{off}$, k_{off}, $10k_{off}$), reveals a qualitative agreement between the measured and anticipated recovery rates ω_{exp} and ω_{theo}, respectively (Figure 6C,D). However, plotting the ratio $\xi = \omega_{exp}/\omega_{theo}$ as a function of k_{off}, where $\omega_{theo} = k_{on} + k_{off}$ is the theoretical recovery rate, one can see that ξ deviates considerably

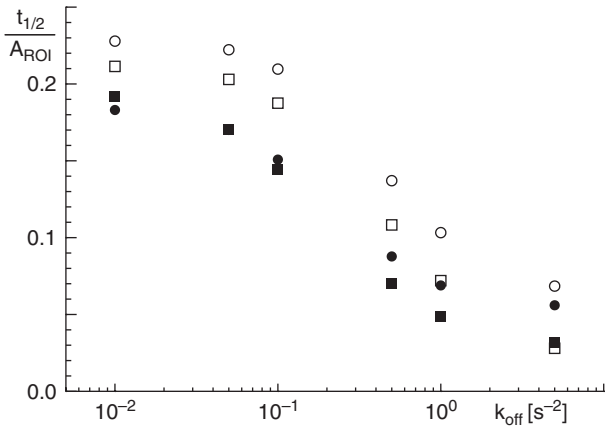

Figure 5: Masked binding kinetics leads to variations of the recovery times with the bleached area. For a purely diffusive recovery, the ratio $t_{1/2}/A_{ROI}$ is expected to be constant for fixed binding kinetics, whereas $t_{1/2}$ should be independent of A_{ROI} for pure binding events (i.e. $t_{1/2}/A_{ROI}$ should decrease). For the uniform binding kinetics in the presence of diffusion (cf. Figure 4, only $k_{on} = k_{off}$), an intermediate behavior is observed. The ratio $t_{1/2}/A_{ROI}$ not only depends on k_{off} but also decreases for increasing A_{ROI} (radius 1.5 μm, 2.5 μm; open, closed symbols). This indicates that the recovery is not only due to diffusion but is also partly mediated by binding events. This result is qualitatively the same for an instantaneous bleaching (□, ■) and at the rate $\gamma = 1/150\,ms^{-1}$ in $n_{iter} = 1$ iterations (○, ●).

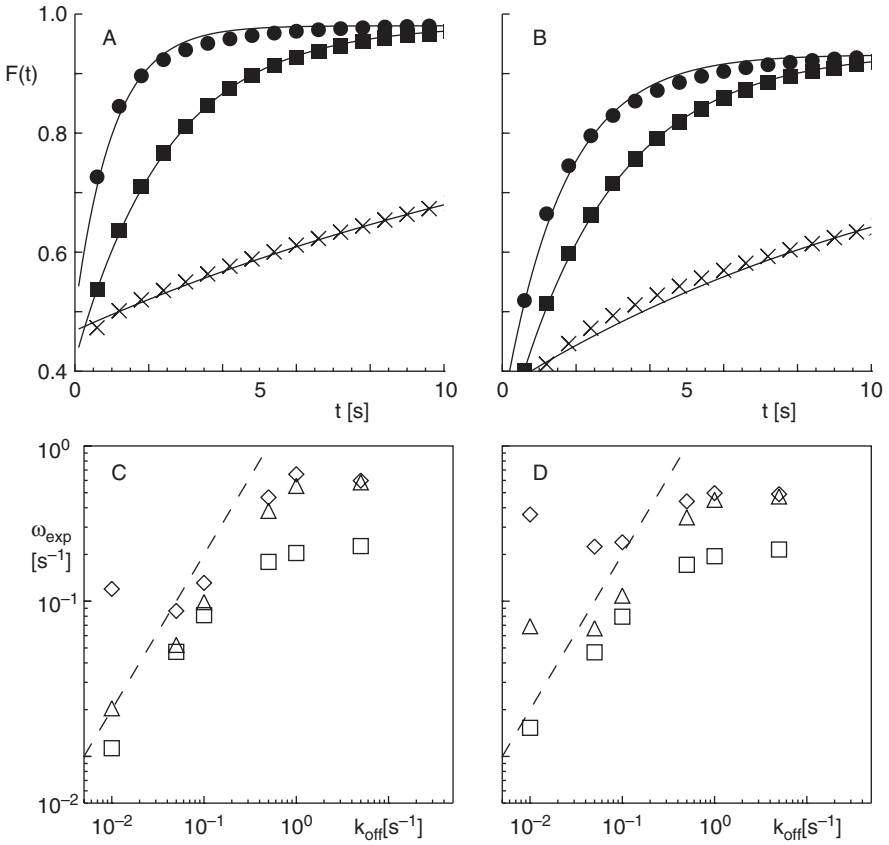

Figure 6: The kinetics of a peripheral membrane protein binding to a 'hot spot' is qualitatively captured by FRAP. A) The recovery after instantaneously bleaching a circular ROI ($r = 2\,\mu m$) is carried by cytoplasmic diffusion ($D_{theo} = 10\ \mu m^2/s$) as well as restricted binding/release to/from to the membrane within the ROI with rates $k_{on} = k_{off} = 0.05/s$ (×), $k_{on} = k_{off} = 0.5/s$ (●) and $k_{on} = k_{off} = 5/s$ (■). In contrast to the scenario in Figure 4, best fits with a model for binding (full lines, eqn. 4) now describe the data well. B) Same as in A when the bleaching was performed with $n_{iter} = 1$ iteration and bleach rate $\gamma = 1/150\,ms^{-1}$. C) Using an instantaneous bleaching, the recovery rate ω_{exp} as obtained by fitting *F(t)* with the model for recovery due to binding (eqn. 4) shows a strong dependence on the imposed binding kinetics (◇: $k_{on} = 0.1k_{off}$, △: $k_{on} = k_{off}$, □: $k_{on} = 10k_{off}$). The dashed line shows the anticipated results ω_{theo} for $k_{on} = k_{off}$. Clearly, the corresponding data for ω_{exp} (triangles) reflect the qualitative behavior of $\omega_{theo,}$ even though the quantitative agreement is still poor (see also Figure 6). D) Same as in C when bleaching with $n_{iter} = 5$ and $\gamma = 1/150\,ms^{-1}$. Please note that the abscissas and ordinates in C and D have a logarithmic scale. Scales on the ordinates are the same within each panel.

from unity for increasing k_{off} (Figure 7). This finding can be understood by considering again the unavoidable (cytoplasmic) diffusional recovery into the ROI. First, the same argument as above applies, i.e. diffusion partially masks the recovery due to binding. Second, the binding becomes diffusion-limited for very fast kinetics, i.e. the diffusive delivery of fluorescent particles to the binding spot limits the binding events. This effect has been reported for the attachment of coatomer to Golgi membranes (19). In other words, one can assess the binding kinetics in many cases

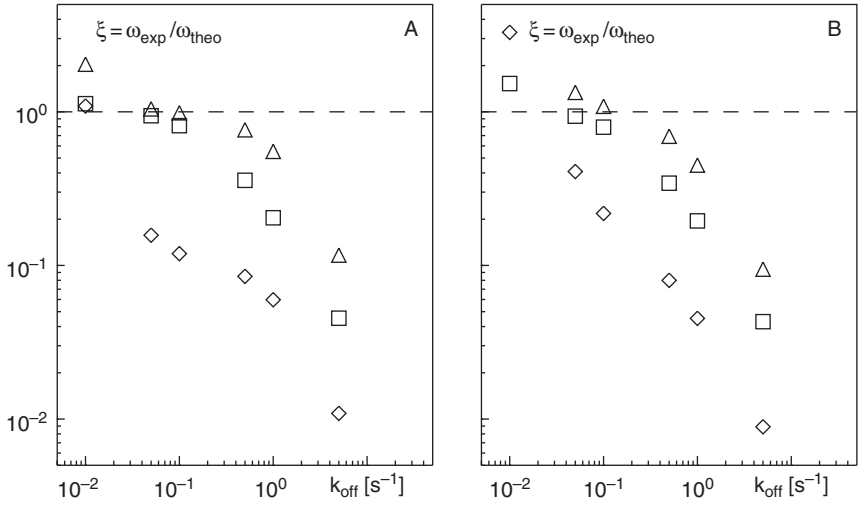

Figure 7: The binding kinetics of peripheral membrane protein to a 'hot spot' is generally underestimated. A) Using an instantaneous bleaching, the ratio $\xi = \omega_{exp}/\omega_{theo}$ deviates from unity when the binding kinetics is fast (◇: $k_{on} = 0.1k_{off}$, △: $k_{on} = k_{off}$, □: $k_{on} = 10k_{off}$). This is due to the fact that diffusion towards the target where binding occurs starts to be limiting and sets the slowest time scale of the recovery. Thus simply fitting the FRAP curve with a fitting function cannot resolve the binding kinetics when diffusion-limited binding kinetics is encountered. B) Same as in A for $n_{iter} = 5$ and $\gamma = 1/150\,ms^{-1}$.

only when considering not only the reaction kinetics but also the diffusion which 'feeds' it.

A 'recipe' to determine the kinetic parameters of binding events is to first determine the diffusional mobilities of the protein of interest (in cytoplasm and on the membrane), e.g. with fluorescence correlation spectroscopy. One can then supplement the FRAP experiments with simulations like the ones presented here, i.e. one takes into account both the diffusion and the binding events. As the diffusion coefficients are known from the previous measurements, the only remaining variable in the simulations is the binding kinetics (k_{on}, k_{off}). Varying these free parameters one can attempt to match the experimental FRAP data and thus determine the kinetic rates.

In conclusion, the interpretation of FRAP curves is highly susceptible to misinterpretation. This holds true for the determination of the diffusional properties of proteins (in the cytoplasm and on membranes), which is hampered by the finite time needed for bleaching the ROI and recording the data. On the other hand, when trying to access the binding kinetics of proteins to membranes, the kinetic parameters may be masked by unavoidable concurrent diffusion events. In view of current efforts to support biological observations with more quantitative modeling approaches (computational/systems biology), there is a clear need for precise data acquisition, e.g. with FRAP. Pattern formation in living cells, for example, can crucially depend on the reaction rates and details of the diffusion of reagents (33). It therefore appears necessary to supplement FRAP measurements with simulations like the ones shown here to improve the evaluation of the data.

Methods

Cell culture and microscopy

Monolayer HeLa cells stably expressing GFP-tagged GalNAc-T2 were cultured as described previously (34). FRAP measurements have been performed on a LSM510 (Carl Zeiss, Jena, Germany) using an Apochromat 40×/1.2 W objective and a 488 nm laser line for illumination; the fluorescence was detected with a bandpass filter [505–550 nm]. The detection gain was chosen such that the ER pool of GalNAc-T2 was almost saturating the dynamic level of the detectors and the pinhole was opened wide enough to collect the fluorescence emerging from all focal planes lying within the cell. With this, the monitored recovery into the bleached circular ROI (radius 2 μm) was essentially carried by a two-dimensional diffusive flux. The data was subsequently fitted using eqn. 2 to determine the diffusion coefficient. During the data acquisition, only the ROI was imaged.

Modeling and simulations

FRAP simulations with purely diffusive recovery were performed by solving the diffusion equation $\frac{\partial C}{\partial t} = D\nabla^2 C$ for the density C of fluorescent particles on a lattice with 220×220 sites and periodic boundary conditions. Discretizing the temporal and spatial derivatives, the diffusion equation for each lattice site (i,j) is given by

$$\frac{C_{i,j}(t+\Delta t) - C_{i,j}(t)}{\Delta t} = D\frac{C_{i-1,j}(t) + C_{i+1,j}(t) + C_{i,j-1}(t) + C_{i,j+1}(t) - 4C_{i,j}(t)}{\Delta x^2}, \quad (1)$$

where $\Delta x = 150$ nm is the lattice spacing and Δt represents the chosen time step. The temporal evolution of this discretized diffusion equation was studied with a 4th order Runge–Kutta scheme (35). Depending on the imposed diffusion coefficient D_{theo}, time steps of 0.1–1 ms were used. For a more extensive introduction to the simulation of differential equations and exemplary codes, the reader is referred to Press et al. (35). A circular ROI with radius $r = 2$ μm in the middle of the lattice was bleached either instantaneously or at rate γ using n_{iter} scanning iterations. To this end, an additional term $-\gamma C_{i,j}(t)$ was added to eqn. 1 for all lattice sites (i,j) inside the ROI during the bleach interval. To match conditions found in real experiments, the time needed to scan the ROI was chosen to be 150 ms. Fitting of the numerically obtained FRAP curves was performed by using the analytically derived fitting function for diffusional recovery into circular regions (6):

$$F(t) = A \cdot e^{-2T/t} \cdot (I_0(2T/t) + I_1(2T/t)) + B \quad (2)$$

Here, I_0, I_1 are modified Bessel functions, B sets the fluorescence directly after the bleaching and $A + B$ determines the saturation value of the recovery. The typical recovery time T is determined by the diffusion coefficient via $T = r^2/(4D)$, that is, by fitting the experimental/numerical data using eqn. 2 one can estimate the diffusion coefficient as

$$D_{exp} = r^2/(4T) \quad (3)$$

The goodness of a fit was quantified by the χ^2-value which measures the deviations of the fit from the data points (35). In most cases, however, the goodness of the fit was already directly observable by visual inspection when superimposing the fit to the data; an example for this is given in Figure 4A,B.

To describe membrane diffusion, a value $D_{theo} = 1$ μm^2/s was typically used in the simulations. This value was chosen because one can calculate an upper bound $D_{theo} = 2.5$ μm^2/s from the Saffman–Delbruck equation (23) when calculating the mobility for a single *trans*-membrane α-helix (radius 0.7 nm) in a typical membrane (thickness 6 nm, viscosity 0.1 kg/(s·m)). A reduction to $D_{theo} = 1$

$\mu m^2/s$ appears reasonable, as the diffusion may be obstructed, e.g. by membrane inhomogeneities.

FRAP simulations with recovery due to binding and diffusion were performed by solving the appropriate reaction–diffusion equation for the density of the membrane-bound and cytoplasmic pools $C^{(m)}$ and $C^{(c)}$ of the labeled particles, e.g. $\frac{\partial C^{(m)}}{\partial t} = k_{on} C^{(c)} - k_{off} C^{(m)} + D\nabla^2 C^{(m)}$ In particular, membrane and cytoplasm were modeled by two interconnected planar lattices ($2 \times 220 \times 220$ sites). While the diffusion in each of the two lattices was discretized analogous to the above approach (cf. eqn. 1), albeit with different diffusion coefficients, the exchange between the lattices was only mediated by the binding/unbinding reaction. This was accomplished by adding a term to $k_{on} C^{(c)}_{i,j} - k_{off} C^{(m)}_{i,j}$ eqn. 1 when describing the 'membrane' lattice and $-k_{on} C^{(c)}_{i,j} + k_{off} C^{(m)}_{i,j}$ when considering the 'cytoplasm' lattice. The lattice spacing was again $\Delta x = 150$ nm and the temporal evolution was obtained with a 4th order Runge–Kutta scheme with periodic boundary conditions in the *xy*-direction. The lower 220×220 lattice represented the cytoplasm and diffusion within this lattice was characterized by an imposed diffusion coefficient $D_{theo} = 10\,\mu m^2/s$, whereas the upper lattice represented the membrane on which diffusion took place with $D_{theo} = 1\,\mu m^2/s$. Binding reactions were allowed to occur either on the entire cytoplasm– membrane interface or were restricted to the ROI. In the latter case, diffusion on the membrane was blocked. As before, a circular ROI with radius $2\,\mu m$ in the center of the superimposed lattices was bleached either instantaneously or with rate γ using n_{iter} scanning iterations. Fitting of the numerically obtained FRAP curves was performed with a formula for recovery due to binding:

$$F(t) = A(1 - exp(-\omega_{exp} t)) + B \qquad (4)$$

The latter is easily derived by neglecting diffusional effects, e.g. diffusion-limited binding (19). Assuming the total number of molecules of the peripheral membrane protein to be C_0 and the membrane bound pool to be C_m, the time course of C_m is given by the ordinary differential equation

$$\frac{dC_m}{dt} = k_{on}(C_0 - C_m) - k_{off} C_m = k_{on} C_0 - (k_{on} + k_{off}) C_m$$

Since the fluorescence F is proportional to the particle number C_m, an equivalent formula holds true for the fluorescence. Solving the differential equation by separation of variables, the theoretical recovery rate is then simply found to be $\omega_{theo} = k_{on} + k_{off}$. It is worthwhile noting here that, in contrast to eqn. 3, the recovery rate ω_{theo} does not depend on the area of the ROI.

Acknowledgments

I would like to thank M. Prummer, M. Elsner and A.C. Rowat for helpful remarks on the manuscript. The MEMPHYS-Center for Biomembrane Physics is supported by the Danish National Research Foundation.

References

1. Axelrod D, Koppel DE, Schlessinger J, Elson E, Webb WW. Mobility measurement by analysis of fluorescence photobleaching recovery kinetics. Biophys J 1976;16:1055–1069.
2. Koppel DE, Axelrod D, Schlessinger J, Elson EL, Webb WW. Dynamics of fluorescence marker concentration as a probe of mobility. Biophys J 1976;16:1315–1329.
3. Weiss M, Nilsson T. In a mirror dimly: tracing the movements of molecules in living cells. Trends Cell Biol 2004;14:267–273.
4. Lippincott-Schwartz J, Snapp E, Kenworthy A. Studying protein dynamics in living cells. Nat Rev Mol Cell Biol 2001;2:444–456.
5. Reits EA, Neefjes JJ. From fixed to FRAP. measuring protein mobility and activity in living cells. Nat Cell Biol 2001;3:E145–E147.
6. Soumpasis DM. Theoretical analysis of fluorescence photobleaching recovery experiments. Biophys J 1983;41:95–97.
7. Aizenbud BM, Gershon ND. Diffusion of molecules on biological membranes of nonplanar form. A theoretical study. Biophys J 1982;38: 287–293.
8. Siggia ED, Lippincott-Schwartz J, Bekiranov S. Diffusion in inhomogeneous media: theory and simulations applied to whole cell photobleach recovery. Biophys J 2000;79:1761–1770.
9. Dayel MJ, Hom EF, Verkman AS. Diffusion of green fluorescent protein in the aqueous-phase lumen of endoplasmic reticulum. Biophys J 1999;76:2843–2851.
10. Olveczky BP, Verkman AS. Monte Carlo analysis of obstructed diffusion in three dimensions: application to molecular diffusion in organelles. Biophys J 1998;74:2722–2730.
11. Partikian A, Olveczky B, Swaminathan R, Li Y, Verkman AS. Rapid diffusion of green fluorescent protein in the mitochondrial matrix. J Cell Biol 1998;140:821–829.
12. Saxton MJ. Anomalous diffusion due to obstacles: a Monte Carlo study. Biophys J 1994;66(2 Part 1):394–401.
13. Saxton MJ. Anomalous diffusion due to binding: a Monte Carlo study. Biophys J 1996;70:1250–1262.
14. Saxton MJ. Anomalous subdiffusion in fluorescence photobleaching recovery: a Monte Carlo study. Biophys J 2001;81:2226–2240.
15. Girod A, Storrie B, Simpson JC, Johannes L, Goud B, Roberts LM, Lord JM, Nilsson T, Pepperkok R. Evidence for a COP-I-independent transport route from the Golgi complex to the endoplasmic reticulum. Nat Cell Biol 1999;1: 423–430.
16. Stephens DJ, Lin-Marq N, Pagano A, Pepperkok R, Paccaud JP. COPI-coated ER-to-Golgi transport complexes segregate from COPII in close proximity to ER exit sites. J Cell Sci 2000;113: 2177–2185.
17. Stephens DJ, Pepperkok R. Imaging of procollagen transport reveals COPI-dependent cargo sorting during ER-to-Golgi transport in mammalian cells. J Cell Sci 2002;115:1149–1160.
18. Presley JF, Ward TH, Pfeifer AC, Siggia ED, Phair RD, Lippincott-Schwartz J. Dissection of COPI and Arf1 dynamics *in vivo* and role in Golgi membrane transport. Nature 2002;417 (6885):187–193.
19. Elsner M, Hashimoto H, Simpson JC, Cassel D, Nilsson T, Weiss M. Spatiotemporal dynamics of the COPI vesicle machinery. EMBO Rep 2003;4:1000–1004.
20. Seksek O, Biwersi J, Verkman AS. Translational diffusion of macromolecule-sized solutes in cytoplasm and nucleus. J Cell Biol 1997;138:131–142.
21. Cole NB, Smith CL, Sciaky N, Terasaki M, Edidin M, Lippincott-Schwartz J. Diffusional mobility of Golgi proteins in membranes of living cells. Science 1996;273 (5276):797–801.
22. Weiss M, Hashimoto H, Nilsson T. Anomalous protein diffusion in living cells as seen by fluorescence correlation spectroscopy. Biophys J 2003;84:4043–4052.

23. Saffman PG, Delbruck M. Brownian motion in biological membranes. Proc Natl Acad Sci U S A 1975;72:3111–3113.
24. Surrey T, Nedelec F, Leibler S, Karsenti E. Physical properties determining self-organization of motors and microtubules. Science 2001;292 (5519):1167–1171.
25. Weiss M, Nilsson T. A kinetic proof-reading mechanism for protein sorting. Traffic 2003;4:65–73.
26. Mogilner A, Oster G. Polymer motors: pushing out the front and pulling up the back. Curr Biol 2003;13:R721–R733.
27. Howard M, Rutenberg AD. Pattern formation inside bacteria: fluctuations due to the low copy number of proteins. Phys Rev Lett 2003;90:128102.
28. Elson EL, Qian H. Interpretation of fluorescence correlation spectroscopy and photobleaching recovery in terms of molecular interactions. Meth Cell Biol 1989;30:307–332.
29. Scales SJ, Pepperkok R, Kreis TE. Visualization of ER-to-Golgi transport in living cells reveals a sequential mode of action for COPII and COPI. Cell 1997;90:1137–1148.
30. Rossanese OW, Soderholm J, Bevis BJ, Sears IB, O'Connor J, Williamson EK, Glick BS. Golgi structure correlates with transitional endoplasmic reticulum organization in *Pichia pastoris* and *Saccharomyces cerevisiae*. J Cell Biol 1999;145:69–81.
31. Elson EL. Fluorescence correlation spectroscopy and photobleaching recovery. Annu Rev Phys Chem 1985;36:379–406.
32. Illenberger D, Walliser C, Strobel J, Gutman O, Niv H, Gaidzik V et al. Rac2 regulation of phospholipase C-beta 2 activity and mode of membrane interactions in intact cells. J Biol Chem 2003;278: 8645–8652.
33. Weiss M. Stabilizing Turing patterns with sub-diffusion in systems with low particle numbers. Phys Rev E 2003;68:036213.
34. Storrie B, White J, Rottger S, Stelzer EH, Suganuma T, Nilsson T. Recycling of golgi-resident glycosyltransferases through the ER reveals a novel pathway and provides an explanation for nocodazole-induced Golgi scattering. J Cell Biol 1998;143:1505–1521.
35. Press WH, Vetterling WT. Numerical recipes in C. The art of scientific computing. Cambridge: Cambridge University Press, 1988.